Title	Three-dimensional seismic velocity tomography of Montserrat from the SEA-CALIPSO offshore/onshore experiment.
Author(s)	Shalev, E.; Kenedi, C. L.; Malin, P.; Voight, V.; Miller, V.; Hidayat, Dannie.; Sparks, R. S. J.; Minshull, T.; Paulatto, M.; Brown, L.; Mattioli, Glen.
Citation	Shalev, E., Kenedi, C. L., Malin, P., Voight, V., Miller, V., Hidayat, D., et al. (2010). Three-dimensional seismic velocity tomography of Montserrat from the SEA-CALIPSO offshore/onshore experiment. Geophysical Research Letters, 37.
Date	2010
URL	http://hdl.handle.net/10220/8808
Rights	

Three-dimensional seismic velocity tomography of Montserrat from the SEA-CALIPSO offshore/onshore experiment

E. Shalev,[1,2] C. L. Kenedi,[1,2] P. Malin,[1,2] V. Voight,[3] V. Miller,[3] D. Hidayat,[3] R. S. J. Sparks,[4] T. Minshull,[5] M. Paulatto,[5] L. Brown,[6] and G. Mattioli[7]

Received 14 January 2010; revised 10 March 2010; accepted 29 March 2010; published 1 May 2010.

[1] The SEA-CALIPSO experiment in December 2007 incorporated a sea-based airgun source, and seismic recorders both on Montserrat and on the adjacent sea floor. A high quality subset of the data was used for a first arrival P-wave velocity tomographic study. A total of more than 115,000 traveltime data from 4413 airgun shots, and 58 recording stations, were used in this high-resolution tomographic inversion. The experiment geometry limited the depth of well resolved structures to about 5 km. The most striking features of the tomography are three relatively high velocity zones below each of the main volcanic centers on Montserrat, and three low velocity zones flanking Centre Hills. We suggest that the high velocity zones represent the solid andesitic cores of the volcano complexes, characterized by wave speeds faster than adjacent volcaniclastic material. The low velocity zones may reflect porous volcaniclastic material and/or alteration by formerly active hydrothermal systems.
Citation: Shalev, E., et al. (2010), Three-dimensional seismic velocity tomography of Montserrat from the SEA-CALIPSO offshore/onshore experiment, *Geophys. Res. Lett.*, *37*, L00E17, doi:10.1029/2010GL042498.

1. Introduction

[2] We present a P-wave velocity tomography study on Montserrat, W.I., based on the SEA-CALIPSO (Seismic Experiment with Airgun-source – Caribbean Andesitic Lava Island Precision Seismo-geodetic Observatory) offshore/onshore active source experiment. Montserrat is a 10 × 16 km volcanic island in the northern half of the Lesser Antilles arc. The Soufrière Hills volcano (SHV) dominates the southern two thirds of the island and has been active and dynamic since July 1995 [*Young et al.*, 1998]. Various lines of evidence have been used to estimate the depth of over 5 km to a magmatic reservoir, including petrology [*Barclay et al.*, 1998], deformation [*Mattioli et al.*, 1998; *Voight et al.*, 2006], and the approximate base of seismic activity [*Aspinall et al.*, 1998]. We attempted to identify the regions of variable velocity under the island, especially under the volcanic centers, and to inquire whether magmatic storage areas could be recognized under the SHV.

2. Seismic Tomography Experiment

[3] The plan was to install a dense array of seismometers on or near the island, and to encircle the island with a ship towing an eight-component GI airgun with a total capacity of 2600 in^3 shooting at 1 minute intervals (B. Voight et al., Active-source seismic experiment reveals structure under Soufriere Hills Volcano, Montserrat, WI, submitted to *Eos Transcations, American Geophysical Union*, 2010). A major focus concerned obtaining high resolution data under the active and hazardous volcano. Since SHV occupies the south-eastern part of the island, most stations were located in safe areas in the north and northwest, and the ship's radial tracks were mostly to the south and east (Figure 1). The short distance between the target zone and the furthest recorder limited the maximum depth of seismic ray penetration below SHV.

[4] Two deployment designs and types of seismic recorders were used on land in SEA-CALIPSO (Voight et al., submittted manuscript, 2010): 29 Reftek 130 recorders, with 3-component Mark Products L22 2 Hz sensors, and 204 Texans (Reftek 125), with single vertical component Mark Products L28 4.5 Hz sensors. In order not to bias the inversion with the closely spaced Texan reflection geometry, only one in ten Texans was included in the tomographic grid.

[5] The seismic network used in the tomographic inversion consisted of 58 stations, including 25 Reftek 130s, 19 Texans, 7 Ocean-Bottom Seismometers (OBSs) with 4.5 Hz sensors, and 7 permanent Montserrat Volcano Observatory (MVO) broadband stations in the exclusion zone. For the duration of the experiment, all instruments recorded continuously, at 250 or 100 samples per second depending on recorder type. The only exception was a subset of six Texans, part of a refraction line in the Belham Valley, that was shut down for several hours mid-experiment for a data quality test.

[6] The data recorded in the experiment was mostly of high quality with easily identifiable first arrivals (Figure 2). Weak signals were recorded from some of the longer ray paths. The first arrivals formed a smooth progression throughout the section; thus, even when a few shots did not show the first arrival, the arrival time could still be identified. In this study we analyzed and picked only the first

[1]Institute of Earth Science and Engineering, University of Auckland, Auckland, New Zealand.
[2]Earth and Ocean Sciences, Duke University, Durham, North Carolina, USA.
[3]Department of Geosciences, Pennsylvania State University, University Park, Pennsylvania, USA.
[4]Department of Earth Sciences, University of Bristol, Bristol, UK.
[5]National Oceanography Centre, University of Southampton, Southampton, UK.
[6]Department of Geosciences, Cornell University, Ithaca, New York, USA.
[7]Department of Geosciences, University of Arkansas, Fayetteville, Arkansas, USA.

0094-8276/10/2010GL042498

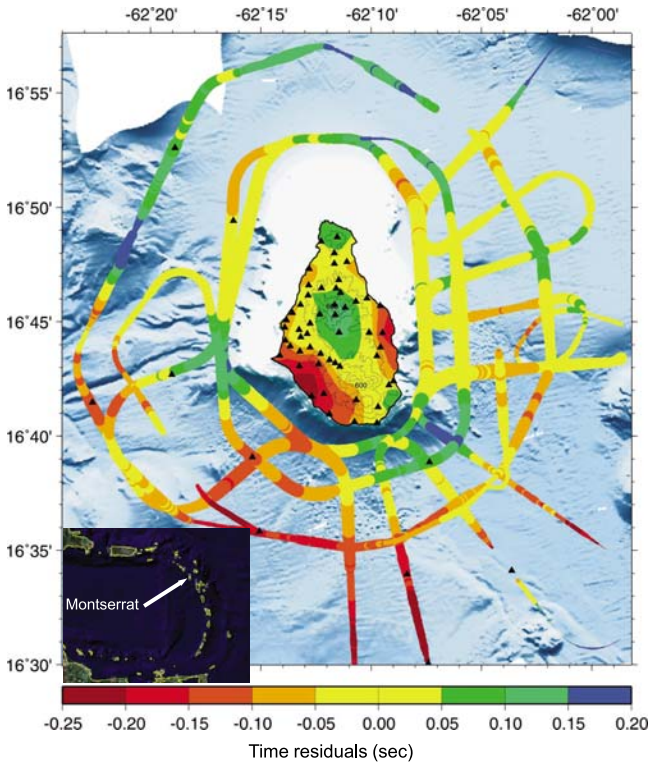

Figure 1. Map of SEA CALIPSO 3D tomography area showing bathymetry, topography contours, ship track, station locations, and average time residuals for shots and land based recorders. Black triangles mark the seismic stations included in the tomographic inversion. The stations offshore are ocean bottom seismometers. Colors stand for the average residuals (time computed minus time observed) in seconds where red represents slow and blue represents fast. On land, the colors contour the average residuals; on water, colors represent the average residual for each shot. The width of the ship track line is proportional to the number of seismic stations that recorded the airgun blast from a particular point on the track.

arrivals and did not use secondary phases. These phases are addressed in other works [*Paulatto et al.*, 2010].

3. Data

[7] The 77 hours of shooting resulted in 4413 shots recorded by 58 stations for a total of 115,158 ray paths. Of all the shots, stations in the north had up to 91% of identifiable first arrivals, while stations around SHV had fewer than 35% identifiable first arrivals due to high attenuation in the younger volcanic deposits. Stations near the coast recorded few first arrivals due to high ambient noise from ocean waves. The data were filtered between 3–15 Hz to correspond with the frequency content of the airgun signal. First arrivals were picked manually and only clear signals were used; thus, uncertainty was assumed to be the same for all first arrivals.

4. Seismic Tomography Method

[8] The first-arrival time data were inverted for a 3D P-wave velocity model of Montserrat and the surrounding ocean using the tomography code from *Shalev and Lees* [1998]. This method uses a Cubic B-spline description of the 3D volume, and the LSQR algorithm to invert the data. This inversion method simultaneously minimized both data misfit and model roughness, which allowed the researcher to choose the desired level of smoothness. The inversion also allowed for station and shot corrections. A separate damping parameter was used for each type of inversion unknown: velocity model, station correction, and shot correction.

[9] Although the 3-D velocity structure extended to 1 km above sea level, ray tracing was computed from sources at sea level to the actual elevation of each station. The length of the water section of each path was assumed to be the depth to the sea floor below each shot. A constant velocity of 1.5 km/s was used to calculate travel time in the water.

[10] We began with a 1D velocity model, using Cubic B-spline interpolation to be consistent with the 3-D inversion. The 1D model for this study was derived from the data using the Levenberg–Marquardt non-linear minimization procedure [*Press et al.*, 1992]. There were two options for the starting velocity model: a) A single starting model for the whole target area, or b) Two starting models, one for land and one for ocean. We tested both types of starting model using the same damping and smoothing parameters, and while the end results were similar, the final RMS of residuals was smaller with two starting models. Therefore, we derived two 1D velocity models, one each for land and for ocean (Figure 2). The boundary between land and ocean was defined as the bathymetric line at 200 m water depth. The derived 1D models differed from the ones used for synthetic ray-path modeling. In particular, the final land model was faster than the ocean model at all depths penetrated by first arrival rays; this resulted in a shallower maximum depth for the turning rays, and reduced the imaging depth.

[11] The total target cube for the 3D inversion (see Figure 1) was 50 × 45 × 8 km. Horizontal velocity grid spacing was 0.5 km in the land area, 1 km for the ocean near the land, and 5 km near the boundaries (see auxiliary material).[1] Vertical grid spacing was 0.5 km to a depth of 5 km, and 1 km below 5 km. A smaller grid spacing of 0.25 km was tested for the center of the land area but showed no improvement.

[12] To check for resolution of the 3D inversion, we ran a checkerboard test based on the starting 1D velocity models. The cell size of the checkerboard was 1.5 × 1.5 × 1.5 km, with the specified variation ±12.5%. A consistent recovery of the pattern was observed to a depth of 4 km in the area of good ray coverage under the island. However, the amplitude of the recovered anomalies was only about two-thirds of the starting amplitude. At 5 km depth, some of the checkerboard anomalies retained their shape but most were blended and smeared. There was no reliable resolution below 5 km depth (see auxiliary material).

[13] Another resolution problem was the tradeoff between station correction and velocity in the top 1 km of the model. The process of allowing for station corrections in the inversion removed most of the variability from the top of the model, and running the inversion without station corrections resulted in a substantially larger residual RMS. The final inversion allows for damped station correction. Nevertheless,

[1] Auxiliary materials are available in the HTML. doi:10.1029/2010GL042498.

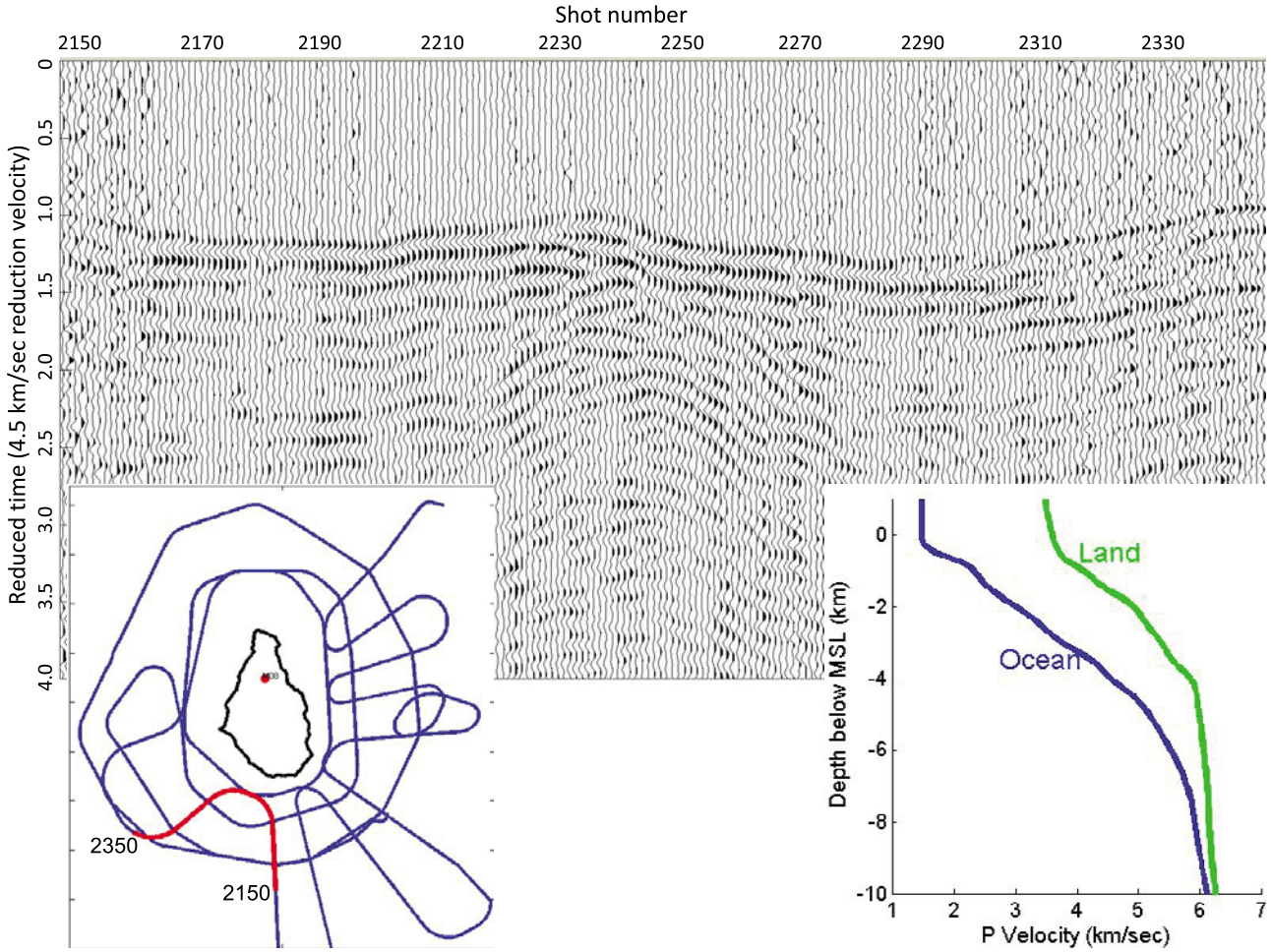

Figure 2. Example of a record section of the vertical component, as recorded by Station M08 on the north slope of Centre Hills, from shots to the southwest of the island. Reduction velocity = 4.5 km/sec. First arrivals are very clear at approximately 1 sec reduced time. Ship path is shown on the left insert in red. 1-D velocity models for land and ocean are shown in right insert.

it is possible that some velocity anomalies in the top 1 km are not imaged because of this compromise.

5. Results

[14] The tomographic inversion converged after 5 iterations. Several sets of damping and smoothing parameters were tested, and the major velocity anomalies were stable regardless of these parameters. The 3D inversion reduced the RMS of the residuals from 167 ms to 80 ms for a variance reduction of 77%. Results of the tomographic inversion are shown in Figures 3 and 4. The maximum lateral variation is about 2 km s^{-1}, which is similar to the results obtained from Deception Island [*Zandomeneghi et al.*, 2009].

[15] The most notable features in the Vp structure are high velocity anomalies below all three volcanic centres of Montserrat at about 2 to 3 km depth. The most prominent of these is the anomaly below Centre Hills, with a similar but less intense anomaly under SHV (Figure 3a). This inversion result was not unexpected, because the average station residual contours in Figure 1 also show positive (fast) residuals for stations near the volcanic centers. The top boundaries of these high velocity anomalies are not clear, due to the tradeoff between station correction and velocity at shallow depth. When the inversion ran without station corrections, the largest fast anomaly under Centre Hills reached the surface, but with higher RMS misfit.

[16] Other large and consistent anomalies are the low velocity regions on the flanks of the volcanic centres. There are three such anomalies to the northeast, northwest, and southwest of Centre Hills. These anomalies are stable regardless of inversion parameters. The east-west cross section (Figure 3d) shows both a high velocity body under SHV and a low velocity anomaly west of SHV. The appearance that the two anomalies are elongated down and away from the center of the island may be an artefact of the rays coming from the perimeter to the center. However, the geometry of the main, high amplitude anomalies of Figure 4 is stable.

6. Discussion

[17] The acquisition geometry of the SEA-CALIPSO tomographic experiment was laid out to target the possible active concentration of magma at >5 km depth under the SHV. The actual seismic velocities beneath and surrounding Montserrat turned out to be faster than expected, thus

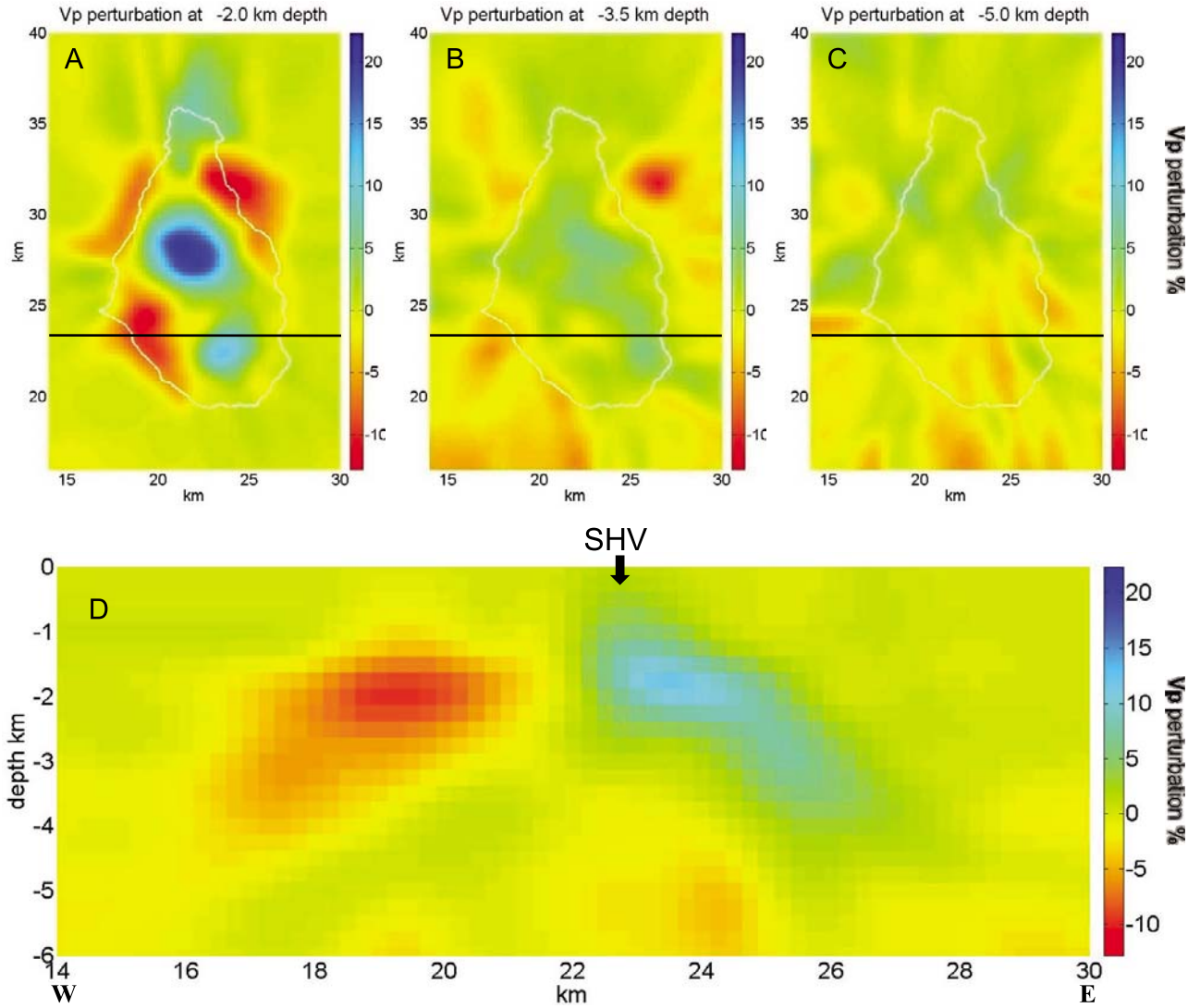

Figure 3. Vp tomography results displayed as perturbation from the average velocity at each depth. Blue represents faster velocities and red represents slower velocities. Map view slices through the target volume at depths (a) 2.0, (b) 3.5, and (c) 5.0 km. The black line marks the location of (d) the cross section across the SHV. The outline of Montserrat is a white line on all map view slices.

turning back most of the refracting seismic energy at depths <5 km. The result was that first-arrival P-wave tomography produced a reliable image of the velocity structure between ~1 and 5 km in depth and extending approximately to the shelf break.

[18] Within this region are six prominent velocity anomalies enclosing perturbations either 6% above or below the average velocities at each depth (Figure 4). Following *Paulatto et al.* [2010], we suggest that the fast anomalies beneath the three constructional volcanic centers may correspond to solid andesitic structural elements in the volcanic cores. The cores would consist of dense, crystallized rock comprising dome cores, sills, dikes, or irregular-shaped intrusions, and adjacent altered zones with silica precipitation, that are seismically faster than the surrounding material, the latter including either lavas from submarine volcano building, and volcaniclastic deposits (talus, block-and-ash flows, lahars etc.). Crystalline cores are consistent with the work of *Harford and Sparks* [2001], who suggest that recurring intrusions solidify at depths up to ~3 km under SHV. This is supported by other evidence that suggests that dikes may rise to 1.5–2 km under SHV, from shallow storage zones [*Mattioli et al.*, 1998; *Hautmann et al.*, 2009; *Voight et al.*, 2010]. It is likely that intrusions have some lateral extent [e.g., *Voight et al.*, 2006], and that considerable volumes of unerupted magma remain in storage zones during the current eruptive activity. The high velocities observed are consistent with nodules found Montserrat-wide as inclusions in eruption products [*Kiddle et al.*, 2010].

[19] The locations of the low-velocity anomalies northeast of Centre Hills and west of SHV suggest a relationship with the volcanic centers and the features may represent syn-volcanic apron deposits. A potential weakness with this hypothesis lies in the fact that these low-velocity features extend to 3–4 km depth. While the weight of the volcano could have been responsible for some degree of crustal flexure and burial of surface material, it cannot easily account for such a depth. There is evidence for buried volcaniclastic

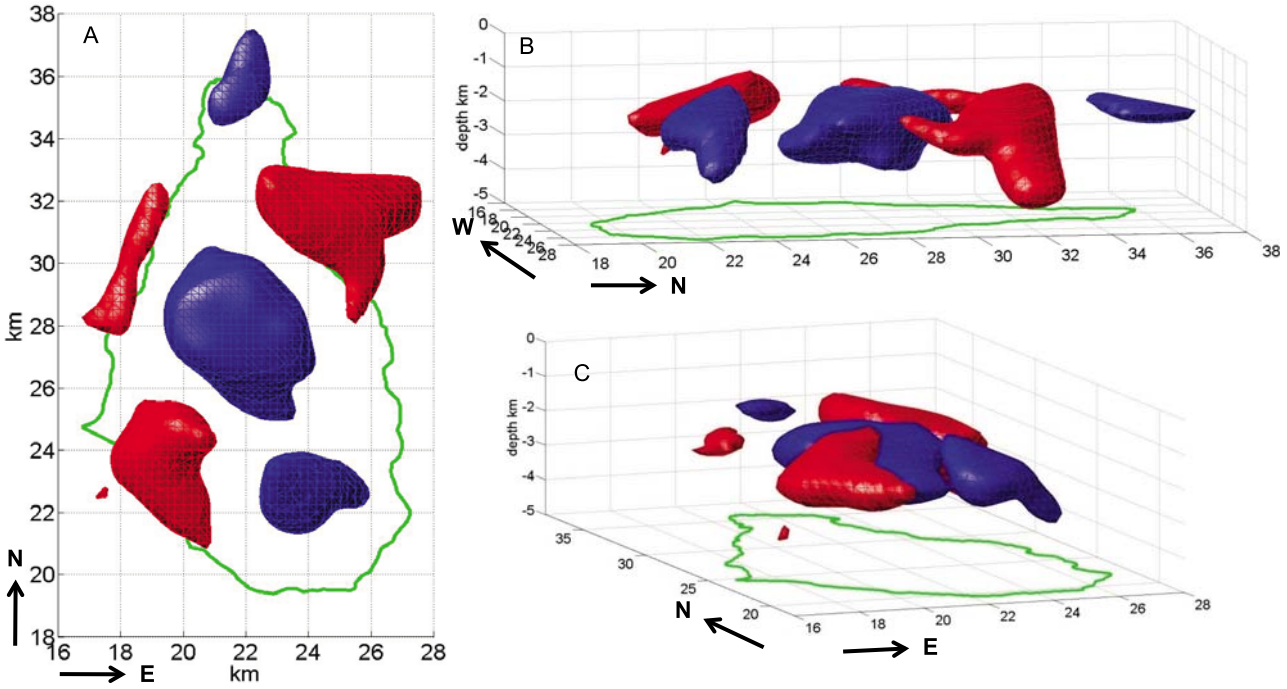

Figure 4. Three-dimensional isosurfaces of velocity anomalies. The blue surfaces define anomalies that are >6% faster than average. The red surfaces represent anomalies that are >6% slower than average. (a) A map view. (b) A view from the east southeast. (C) A view from the south southwest.

fan deposits at 1.5–2 km depth off the east coast of Montserrat (C. L. Kenedi et al., Active faulting and oblique extension influence volcanism on Montserrat (West Indies): Evidence from offshore seismic reflection profiles, manuscript in preparation, 2010).

[20] Another possibility is that the low-velocity features result from hydrothermal alteration, shown to lower seismic velocities in oceanic rocks [*Carlson*, 2001]. Evidence for hydrothermal circulation beneath the Garibaldi-Richmond-St. Georges Hills includes anomalous seismic activity [*Rowe et al.*, 2004], as well as surface hot springs, hot water in boreholes, and a warm pond near Richmond Hill [*Chiodini et al.*, 1996]. Tectonic faulting in the Belham Valley (Kenedi et al., manuscript in preparation, 2010) may be related to this hydrothermal activity. Hydrothermally altered rocks occur at the surface in parts of the Silver Hills (B. Voight, unpublished observations, 2003). A recent MT study on Montserrat shows good correlation between these low velocity zones and low resistivity at 1–4 km depth (G. Ryan, personal communication, 2009). Hydrothermal alteration due to geothermal fluid circulation is a frequent phenomenon in volcanic areas, and geothermal systems are commonly several km in diameter, approximately the size of the low-velocity anomalies in Montserrat. The position of the three low-velocity anomalies around Centre Hills may suggest that geothermal activity was more prevalent about 1–0.4 Ma, when Centre Hills was active.

[21] **Acknowledgments.** We thank the National Science Foundation Continental Dynamics, Geophysics, and Instrumentation & Facilities Programs, the British Geological Survey, Discovery Channel TV, and the British Foreign & Commonwealth Office for funding the SEA-CALIPSO project, the IRIS PASSCAL Instrument Center for providing instrumentation and technical support for the project, and the many people who worked hard aboard the ship or on land to deploy instruments and collect seismic data during December 2007. Thanks also to the good people of Montserrat who allowed us the use of their properties for instrument deployment.

References

Aspinall, W. P., A. D. Miller, L. L. Lynch, J. L. Latchman, R. C. Stewart, R. A. White, and J. A. Power (1998), Soufrière Hills eruption, Montserrat, 1995–1997: Volcanic earthquake locations and fault plane solutions, *Geophys. Res. Lett.*, *25*(18), 3397–3400, doi:10.1029/98GL00858.

Barclay, J., M. J. Rutherford, M. R. Carroll, M. D. Murphy, J. D. Devine, J. Gardner, and R. S. J. Sparks (1998), Experimental phase equilibria constraints on pre-eruptive storage conditions of the Soufrière Hills magma, *Geophys. Res. Lett.*, *25*(18), 3437–3440, doi:10.1029/98GL00856.

Carlson, R. L. (2001), The effects of temperature, pressure, and alteration on seismic properties of diabase dike rocks from DSDP/ODP Hole 504B, *Geophys. Res. Lett.*, *28*(20), 3979–3982, doi:10.1029/2001GL013426.

Chiodini, G., R. Cioni, A. Frullani, M. Guidi, L. Marini, F. Prati, and B. Raco (1996), Fluid geochemistry of Montserrat Island, West Indies, *Bull. Volcanol.*, *58*, 380–392, doi:10.1007/s004450050146.

Harford, C. L., and R. S. J. Sparks (2001), Recent remobilization of shallow-level intrusions on Montserrat revealed by hydrogen isotope composition of amphiboles, *Earth Planet. Sci. Lett.*, *185*, 285–297, doi:10.1016/S0012-821X(00)00373-3.

Hautmann, S., J. Gottsmann, R. S. J. Sparks, A. Costa, O. Melnik, and B. Voight (2009), Modeling ground deformation caused by oscillating overpressure in a dyke conduit at Soufrière Hills Volcano, Montserrat, *Tectonophysics*, *471*, 87–95, doi:10.1016/j.tecto.2008.10.021.

Kiddle, E. J., B. R. Edwards, S. C. Loughlin, M. Petterson, R. S. J. Sparks, and B. Voight (2010), Crustal structure beneath Montserrat, Lesser Antilles, constrained by xenoliths, seismic velocity structure and petrology, *Geophys. Res. Lett.*, *37*, L00E11, doi:10.1029/2009GL042145.

Mattioli, G. S., T. H. Dixon, F. Farina, E. S. Howell, P. E. Jansma, and A. L. Smith (1998), GPS measurement of surface deformation around Soufrière Hills Volcano, Montserrat from October 1995 to July 1996, *Geophys. Res. Lett.*, *25*(18), 3417–3420, doi:10.1029/98GL00931.

Paulatto, M., et al. (2010), Upper crustal structure of an active volcano from refraction/reflection tomography, Montserrat, Lesser Antilles, *Geophys. J. Int.*, *180*(2), 685–696, doi:10.1111/j.1365-246X.2009.04445.x.

Press, W. H., S. A. Teukolsky, W. T. Vetterling, and B. P. Flannery (1992), *Numerical recipes in C: The Art of Scientific Computing*, 2nd ed., Cambridge Univ. Press, New York.

Rowe, C. A., C. H. Thurber, and R. A. White (2004), Dome growth behavior at Soufrière Hills Volcano, Montserrat, revealed by relocation of volcanic event swarms, 1995–1996, *J. Volcanol. Geotherm. Res.*, *134*(3), 199–221, doi:10.1016/j.jvolgeores.2004.01.008.

Shalev, E., and J. M. Lees (1998), Cubic B-splines tomography at Loma Prieta, *Bull. Seismol. Soc. Am.*, *88*, 256–269.

Voight, B., et al. (2006), Unprecedented pressure increase in deep magma reservoir triggered by lava-dome collapse, *Geophys. Res. Lett.*, *33*, L03312, doi:10.1029/2005GL024870.

Voight, B., C. Widiwijayanti, G. Mattioli, D. Elsworth, D. Hidayat, and M. Strutt (2010), Magma-sponge hypothesis and stratovolcanoes: Case for a compressible reservoir and quasi-steady deep influx at Soufrière Hills Volcano, Montserrat, *Geophys. Res. Lett.*, *37*, L00E05, doi:10.1029/2009GL041732.

Young, S. R., R. S. J. Sparks, R. Robertson, L. Lynch, A. D. Miller, J. B. Shepherd, and W. A. Aspinall (1998), Overview of the Soufrière Hills volcano and the eruption, *Geophys. Res. Lett.*, *25*(18), 3389–3392, doi:10.1029/98GL01405.

Zandomeneghi, D., A. Barclay, J. Almendros, J. M. Ibañez Godoy, W. S. D. Wilcock, and T. Ben-Zvi (2009), Crustal structure of Deception Island volcano from *P* wave seismic tomography: Tectonic and volcanic implications, *J. Geophys. Res.*, *114*, B06310, doi:10.1029/2008JB006119.

L. Brown, Department of Geosciences, Cornell University, 2146 Snee Hall, Ithaca, NY 14853, USA.

D. Hidayat, V. Miller, and B. Voight, Department of Geosciences, Pennsylvania State University, 540 Deike Bldg., University Park, PA 16802, USA.

C. L. Kenedi, P. Malin, and E. Shalev, Institute of Earth Science and Engineering, University of Auckland, Private Bag 92019, Auckland 1142, New Zealand. (e.shalev@auckland.ac.nz)

G. Mattioli, Department of Geosciences, University of Arkansas, 113 Ozark Hall, Fayetteville, AR 72701, USA.

T. Minshull and M. Paulatto, National Oceanography Centre, University of Southampton, European Way, Southampton SO14 3ZH, UK.

R. S. J. Sparks, Department of Earth Sciences, University of Bristol, Wills Memorial Building, Queen's Road, Bristol BS8 1RJ, UK.